Explicit solutions of a convection-reaction equation and defects of difference schemes

Youngsoo Ha [a] and Yong Jung Kim [a,*]

[a] *Division of Applied Mathemtics, KAIST (Korea Advanced Institute of Science and Technology), 373-1 Gusong-dong, Yusong-gu, Taejon, 305-701, South Korea*

Abstract

We introduce two kinds of explicit solutions to the convection-reaction equation,

$$u_t + (|u|^q/q)_x = u, \qquad u, x \in \mathbf{R},\ t \in \mathbf{R}^+,\ q > 1,$$

and employ them to test properties of various computational schemes. From this test we observe that computed solutions using Lax-Friedrichs, MacCormack and Lax-Wendroff schemes break down in a finite time. On the other hand some other schemes including WENO, NT and Godunov show more stable behavior and the tests provide their detailed behaviors. It is discussed that if a numerical scheme is applied to this problem together with the splitting method, certain defects of the scheme can be magnified exponentially and observed easily. Sometimes such a behavior destroys the numerical solution completely and hence one need to pay extra caution to deal with reaction dominant systems.

Contents

* Corresponding author, Tel: +82-42-869-2739, Fax: +82-42-869-5710
Email addresses: young@amath.kaist.ac.kr (Youngsoo Ha), ykim@amath.kaist.ac.kr (Yong Jung Kim).

1 Introduction

The scientific computation for the solutions of systems of hyperbolic conservation laws has been successful thanks to the development of accurate numerical schemes (see [2,12,19,20] for example). The unfortunate situation we still have here is that there is no meaningful progress in the analysis of such schemes due to their complexity and it is hard to find any useful error estimate. Furthermore, each scheme has features quite its own and produces numerical results that require proper interpretations. For example, Figures 4.7 and 4.8 in [14] show quite different characters of each schemes considered and it is hard to decide which one is more physically meaningful. Therefore, it is desirable to know the qualitative properties of schemes since one is always forced to choose a proper scheme to a specific problem under consideration.

The main goal of this paper is to develop a method to survey the property of numerical schemes. Our method starts with a Cauchy problem for a convection-reaction equation

$$u_t + uu_x = u, \quad u(x,0) = u_0(x) \in L^1(\mathbf{R}). \tag{1.1}$$

This equation models the roll wave [7] and several analytic properties have been studied in [8,16]. We introduce a more general case (2.1) by considering the flux function as a general convex power law (2.2). In Section 2 we derive two kinds of explicit solutions of the problem, (2.8) and (2.11), which enable us to compare computed solutions with an exact one.

The linear reaction term plays the role of a source which produces an exponential growth. One of the simplest way to treat this source term is a fractional step splitting method which is discussed in Section 3. The main advantage of employing the splitting method in this paper is that the defects of the scheme are magnified exponentially (see Proposition 1) which serves our main goal of this work.

In the rest of the paper several numerical schemes are tested comparing with the exact solutions of the convection-reaction equation (2.1). In Sections 4 and 5 we examine the Lax-Friedrichs, the MacCormack's and the Lax-Wendroff schemes. It is quite surprising that these three well known schemes show unexpected behaviors and the computed solutions break down in a finite time (see Figures 1–5). As mentioned the source of these strange behavior is not

from splitting method but from the numerical schemes for the convection. This observation shows that a small undesired defect of the scheme can be simply magnified and finally destroy the computed solution completely. These examples indicate that one need should take extra caution to deal with a reaction dominant system.

Note that one may consider a method to handle the source term in a way that such a defect of the scheme is neutralized but not magnified. For that purpose the convection-reaction equation (2.1) can be used as a simple model equation. One may also modify the scheme curing the symptoms observed. However the goal of this paper is simply to survey the property of numerical schemes and hence such possibilities are not pursued here.

In Sections 6, 7 and 8 several other schemes such as NT, NTK, Godunov and WENO schemes are tested. These schemes do not show such bizarre behaviors observed previously and hence we could survey their properties in detail. The first test is for the accuracy of the shock location of computed solutions. In this study the second order Godunov scheme showed the most excellent performance among others (see Figures 15 and 16). Even the first order one showed better results than others for certain cases.

The other test is to compute the roll wave given explicitly by (2.11), which shows clearly how does a scheme approximate the rarefaction wave. In this study the approximation error given by (6.5) is an increasing function away from shock discontinuities (see the second row of Figure 8 for example). The only exceptions are the first and the second order Godunov schemes, Figures 14 and 17. For certain cases the error function decreases which means that the Godunov scheme gave slightly overestimated numerical flux for the cases.

2 Exact solutions

We consider the entropy solution of a scalar conservation law with a linear source term

$$u_t + f(u)_x = u, \quad u(x,0) = u_0(x) \in L^1(\mathbf{R}), \qquad x, u \in \mathbf{R}, \quad t > 0, \quad (2.1)$$

where the flux is given by the convex power law

$$f(u) = \frac{1}{q}|u|^q, \qquad q > 1. \quad (2.2)$$

Since the flux considered is convex, $f''(u) \geq 0$, the entropy solution is simply the one that satisfies

$$u(x-) \geq u(x+), \qquad \text{for all} \quad x \in \mathbf{R}. \tag{2.3}$$

Under the change of variables

$$w = e^{-t/q}u, \quad \xi = e^{(1-q)t/q}x, \tag{2.4}$$

one can easily check that the convection-reaction equation (2.1) is transformed to

$$w_t + \frac{1}{q}(|w|^q - (q-1)\xi w)_\xi = 0, \quad w(\xi, 0) = u_0(\xi). \tag{2.5}$$

Consider a time independent function

$$\mathcal{W}_{a,b}(\xi) = \begin{cases} g(\xi) \ , \ -a < \xi < b, \\ 0 \quad , \ \text{otherwise}, \end{cases} \tag{2.6}$$

where $a, b \geq 0$ and the function $g(\xi)$ is the rarefaction profile given by

$$g(\xi) = \text{sign}(\xi) \sqrt[q-1]{(q-1)|\xi|}\,. \tag{2.7}$$

Then $\mathcal{W}_{a,b}$ is clearly a piecewise smooth function that satisfies the entropy condition (2.3) everywhere and the equation (2.5) piecewise. Furthermore, one can easily compute that the discontinuities at $x = -a$ and $x = b$ are stationary using the Rankine-Hugoniot jump condition. Therefore, $w(\xi, t) = \mathcal{W}_{a,b}(\xi)$ is a steady solution of (2.5). If we return to the original variables, then we may obtain our first explicit solution of (2.1), which is a time dependent N-wave:

$$\mathcal{N}_{a,b}(x,t) = \begin{cases} g(x) \ , \ -ae^{(q-1)t/q} < x < be^{(q-1)t/q}, \\ 0 \quad , \qquad\qquad \text{otherwise}. \end{cases} \tag{2.8}$$

Notice that the support of this explicit solution grows exponentially in time. Consider another set of variables:

$$v = e^{-t}u, \quad s = \frac{1}{q-1}\Big(e^{(q-1)t} - 1\Big). \tag{2.9}$$

Then the convection-reaction equation (2.1) is transformed to the usual scalar conservation law:

$$v_s + f(v)_x = 0, \quad v(x,0) = u_0(x). \tag{2.10}$$

The behavior of this homogeneous conservation law is well understood. One of the simplest case is that when the initial value is given by rarefaction waves. Suppose that the initial value is given by so called a roll wave:

$$\mathcal{R}_1(x) = \begin{cases} g(x+1) \ , & -1 < x < 0, \\ g(x-1) \ , & 0 < x < 1, \\ \quad 0 \quad , & \text{otherwise.} \end{cases} \tag{2.11}$$

Then, the solution of (2.10) is given explicitly by two rarefaction waves centered at $x = 1$ and $x = -1$ and a stationary shock wave at $x = 0$. If we return back to the original variable, then we may check that the roll wave in (2.11) is a steady solution of (2.1), which is our second explicit solution. We can also check that it is a piecewise smooth solution with zero shock speed satisfying the entropy condition (2.3).

Notice that there is a sensitivity issue related to steady states. To see such a structure consider the total mass $M(t) = \int u(x,t)dx$. Then its derivative is

$$\frac{d}{dt}M(t) = \frac{d}{dt}\int u dx = \int u_t dx = -\int f(u)_x dx + \int u dx = M(t).$$

Therefore, the total mass M grows exponentially,

$$M(t) = M(0)e^t \tag{2.12}$$

and hence all the integrable steady states should have exactly zero total mass. The roll wave in (2.11) is the case. However, even a small deviation such as rounding off errors will grow exponentially and the solution will diverge eventually. Therefore a numerical computation for the steady state is meaningful only for a certain period of time depending on the precision of the computation.

In the rest of this paper these explicit solutions are used to test properties of several numerical schemes.

3 Splitting Method

In numerical computations a convection-reaction equation such as (2.1) is usually treated by a fractional step splitting method, in which one alternates between solving the convection equation

$$u_t + f(u)_x = 0 \tag{3.1}$$

and the ordinary differential equation

$$u_t = u \tag{3.2}$$

in each time step. First we introduce our notations. Consider a uniform mesh points $x_{j+1/2}$ and a fixed width $\Delta x > 0$, where $x_{j+1/2} = (j + 1/2)\Delta x$, $j \in \mathbf{Z}$. Since the actual wave speed of an N-wave type solution increases exponentially in time, the time step $\Delta t^n := t^{n+1} - t^n, n = 0, 1, \cdots$, and time mesh $t^n = \sum_{k=0}^{n-1} \Delta t^k$ are decided by setting the CFL number to a constant $0 < \nu \leq 1$, i.e.,

$$\frac{\Delta t^n}{\Delta x} f'(\tilde{u}_n) = \nu, \tag{3.3}$$

where $\Delta x/\Delta t^n$ is the numerical wave speed, and $\tilde{u}_n$ is the maximum of the exact solution, $\tilde{u}_n = \max_x |u(x, t^n)|$. In the case that the exact solution is unknown this maximum is usually replaced by the maximum of its approximation $\max_j |U_j^n|$. However, in our case the exact solution is given explicitly by the formula (2.8) and (2.11) and hence the maximum $\tilde{u}_n = \max_x |u(x, t^n)|$ is easily obtained. We view the approximation U_j^n as the cell average of the true solution, i.e.,

$$U_j^n \simeq \frac{1}{\Delta x} \int_{x_{j-1/2}}^{x_{j+1/2}} u(x, t^n) dx. \tag{3.4}$$

We also view $u_{j+1/2}^n$ as the approximation of $u(x, t)$ at the interface $x_{j+1/2}$ of each cells. In a conservative numerical scheme the interface $u_{j+1/2}^n$ is approximated from its neighboring cell averages and we may set

$$u_{j+1/2}^n \equiv I(U_{j-p}^n, \cdots, U_{j+q}^n) \sim u(x_{j+1/2}, t), \qquad t^n \leq t \leq t^{n+1}. \tag{3.5}$$

Then, after integrating (3.1) over the mesh $[x_{j-1/2}, x_{j+1/2}]$, we obtain

$$\frac{\partial}{\partial t}(U_j^n) = \frac{f(u_{j-1/2}^n) - f(u_{j+1/2}^n)}{\Delta x} \equiv \mathcal{L}(U^n; j). \tag{3.6}$$

Note that in many numerical schemes an approximation of the flux at the interface, $f(u^n_{j+1/2})$, is considered instead of the interface approximation, $u^n_{j+1/2}$, itself. In either cases the numerical scheme is based on (3.6) and the operator $\mathcal{L}$ is well defined.

For the time discretization we mostly employ the forward time difference,

$$\bar{U}^{n+1}_j = U^n_j + \frac{\Delta t^n}{\Delta x}\Big(f(u^n_{j-1/2}) - f(u^n_{j+1/2})\Big) (= U^n_j + \Delta t^n \mathcal{L}(U^n; j)\ ), \quad (3.7)$$

which completes the computation of the first part (3.1). On the other hand the ordinary differential equation (3.2) can be exactly solved and we obtain

$$U^{n+1}_j = e^{\Delta t^n} \bar{U}^{n+1}_j. \quad (3.8)$$

Combining these two steps we obtain a fully discrete numerical scheme

$$U^{n+1}_j = e^{\Delta t^n}\Big(U^n_j - \frac{\Delta t^n}{\Delta x}(f(u^n_{j+1/2}) - f(u^n_{j-1/2}))\ \Big). \quad (3.9)$$

Notice that the second equation (3.2) is treated exactly and hence the numerical error will be caused from the first step (3.7) only. Since the focus of this paper is to study the behavior of the numerical schemes such as (3.7), this approach serves our goal well.

We may employ a 3rd-order TVD Runge-Kutta discretization for time stepping (see [18]). In the case the scheme is written as

$$\begin{aligned} U^{(1)}_j &= U^n_j + \Delta t^n \mathcal{L}(U^n; j) \\ U^{(2)}_j &= \frac{3}{4}U^n_j + \frac{1}{4}U^{(1)}_j + \frac{1}{4}\Delta t^n \mathcal{L}(U^{(1)}; j) \\ U^{n+1}_j &= e^{\Delta t^n}\Big(\frac{1}{3}U^n_j + \frac{2}{3}U^{(2)}_j + \frac{2}{3}\Delta t^n \mathcal{L}(U^{(2)}; j)\Big), \end{aligned} \quad (3.10)$$

where the finite difference operator $\mathcal{L}$ is given by (3.6). This kind of semi-discrete schemes usually provide better performance than the fully discrete methods (3.9). However the unexpected behaviors of schemes presented in this paper are observed from both of fully and semi discrete methods.

Finally, we provide a proposition which indicates that any unexpected behavior of the numerical approximation based on (3.9) is just a mirror image of such a behavior of the numerical scheme (3.7) for the convection equation (3.1).

Proposition 1 *Let $V_j^n \sim v(x, s^n)$ be the approximation of the solution to the homogeneous problem (2.10) obtained by the scheme*

$$V_j^{n+1} = V_j^n - \frac{\Delta s^n}{\Delta x}(f(v_{j+1/2}^n) - f(v_{j-1/2}^n)), \ \frac{\Delta s^n}{\Delta x} f'(\max_x |v(x, s^n)|) = \nu,$$

where $\Delta s^n = s^{n+1} - s^n$, $0 < \nu < 1$ is a fixed CFL number, and v is the exact solution of (2.10). If the interface approximation (3.5) satisfies

$$I(CU_{j-p}, \cdots, CU_{j+q}) = CI(U_{j-p}, \cdots, U_{j+q}), \quad C > 0, \tag{3.11}$$

then the approximation $U_j^n \sim u(x, t^n)$ given by (3.9) with (3.3) satisfy

$$U_j^n = e^{t^n} V_j^n \quad \textit{for any} \quad n \geq 0. \tag{3.12}$$

PROOF. We use inductive arguments. The relation (3.12) holds for $n = 0$ since U_j^0 and V_j^0 are the initial discretization of the same initial value $u_0(x)$. Now we show (3.12) for $n+1$ assuming that it holds for n. Let $U_j^n = CV_j^n$ by setting $C = e^{t^n}$. Then the relation between Δt^n and Δs^n is given by

$$\Delta t^n = \frac{\nu \Delta x}{f'(\max_x |u(x, t^n)|)} = \frac{\nu \Delta x}{f'(\max_x |Cv(x, t^n)|)} = \frac{\nu \Delta x}{C^{q-1} f'(\max_x |v(x, t^n)|)} = \frac{\Delta s^n}{C^{q-1}},$$

where ν is the fixed CFL number. Then under the assumption on the interface approximation (3.11) the numerical scheme (3.9) becomes

$$\begin{aligned} U_j^{n+1} &= e^{\Delta t^n} \Big(CV_j^n - \tfrac{\Delta s^n}{C^{q-1}\Delta x}(f(Cv_{j+1/2}^n) - f(Cv_{j-1/2}^n)) \Big) \\ &= e^{\Delta t^n} C \Big(V_j^n - \tfrac{\Delta t^n}{\Delta x}(f(v_{j+1/2}^n) - f(v_{j-1/2}^n)) \Big) = e^{t^{n+1}} V_j^{n+1}, \end{aligned} \tag{3.13}$$

which implies (3.12) for $n+1$. $\square$

Notice that the relation between V_j^n and U_j^n in (3.12) exactly reflects the change of variable $u = e^t v$ in (2.9). The second part of the change of variable for the time variable is not immediate. However, assuming Δt^n's are constant and small, $\Delta t^n = k \ll 1$, we can easily check that

$$s^n = k_1' + \cdots k_{n-1}' = \sum_{i=0}^{n-1} e^{i(q-1)k} k \sim \int_0^{t^n} e^{(q-1)t} dt = \frac{1}{q-1}\Big(e^{(q-1)t^n} - 1 \Big),$$

which approximates the other half of the change of variables in (2.9).

The assumption (3.11) on the interface approximation is natural since it only implies that the interface approximation of $Cu(x, t)$ should be simply C times

the interface approximation of $u(x,t)$. One can easily check that the interface of the Godunov method (7.1) clearly satisfies this interface assumption.

However, unfortunately, most of other schemes do not satisfy this assumption. It seems that, if a numerical scheme is consistent, this assumption should be satisfied up to the leading order (see an example in Section 5). Furthermore, for the Lax-Friedrichs scheme, the assertion (3.12) of the proposition holds (see Section 4).

Finally we discuss about initial values. In this paper we consider three kinds of exact solutions discussed in Section 2. The first example comes with a positive initial value $u(x,0) = \mathcal{N}_{0,1}(x,0)$. Then the exact solution is the positive N-wave

$$u(x,t) = \mathcal{N}_{0,1}(x,t), \tag{3.14}$$

which is given explicitly by (2.8). Since the numerical approximation is for the cell average (3.4), the discretization of the initial data is taken as

$$U_j^0 := \frac{1}{\Delta x} \int_{x_{j-1/2}}^{x_{j+1/2}} \mathcal{N}_{0,1}(x,0)dx. \tag{3.15}$$

In the second example the initial value is given by $u(x,0) = \mathcal{N}_{1,1}(x,0)$ which has both of negative and positive parts. Then the exact solution is the sign-changing N-wave

$$u(x,t) = \mathcal{N}_{1,1}(x,t). \tag{3.16}$$

We may take the initial discretization in the same way as in (3.15). Let $P(t) = \int_0^\infty u(x,t)dx$ which give the total mass of the positive part. Then as we obtained (2.12) we can easily show

$$P(t) = P(0)e^t.$$

This shows the sensitivity of the wave propagation on the initial discretization. We want to assign U_j^0 the same sizes of positive and negative parts as those of the initial value and hence take

$$U_j^0 := \frac{1}{\Delta x} \int_{x_j}^{x_{j+1}} \mathcal{N}_{1,1}(x,0)dx. \tag{3.17}$$

In this way we may remove all the other source of computation error and observe the properties of numerical schemes. We may observe that some nu-

merical schemes provide the shock place equally well for both of the cases. However, some schemes show poor approximation for a sign-changing case.

The initial value of the last example is the roll wave $u(x,0) = \mathcal{R}_1(x)$. We consider the problem under a periodic boundary condition, $u(x,t) = u(x+2,t)$, $t > 0$. Then the exact solution is the time invariant roll wave,

$$u(x,t) = \mathcal{R}_1(x), \qquad -1 < x < 1,\ t > 0. \tag{3.18}$$

The initial value is discretize in the same manner as the one in (3.17) that is

$$U_j^0 := \frac{1}{\Delta x} \int_{x_j}^{x_{j+1}} \mathcal{R}_1(x)dx. \tag{3.19}$$

We may also consider initial discretization of type the (3.17) for this example. In the case same phenomena are observed. The difference is specific properties of numerical schemes are reduced due to the extra zero points which suppress the solution at the boundary. Since our goal is to observe the property of numerical schemes we employ (3.19). This example is particularly good to observe how does the scheme approximates rarefaction waves.

To test properties of numerical schemes we also consider three different powers in the flux function, which are $q = 1.5, 2$ and 3. In the following sections we have selected a few examples from these nine possible cases which show interesting properties of each schemes. A more comprehensive list of numerical examples can be found in [3].

4 Lax-Friedrichs (LxF) type schemes

In this section we consider the Lax-Friedrichs (LxF for short) scheme and its second order modification. The numerical flux of the LxF scheme at the interface $x_{j+1/2}$ is given by

$$f(u_{j+1/2}^n) = \frac{\Delta x}{2\Delta t^n}(U_j^n - U_{j+1}^n) + \frac{1}{2}(f(U_j^n) + f(U_{j+1}^n)). \tag{4.1}$$

Then the numerical scheme (3.9) is written as

$$U_j^{n+1} = e^{\Delta t^n}\Big(\frac{1}{2}(U_{j+1}^n + U_{j-1}^n) - \frac{\Delta t^n}{2\Delta x}(f(U_{j+1}^n) - f(U_{j-1}^n))\ \Big). \tag{4.2}$$

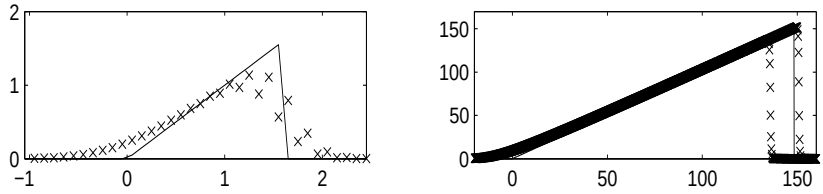

$t = 1$ $t = 10$

Fig. 1. LxF Scheme (4.2) for the positive solution (3.14) with $q = 2$. The computed solution evolves into two separated N-waves. ($\times : Numerical, - : exact$).

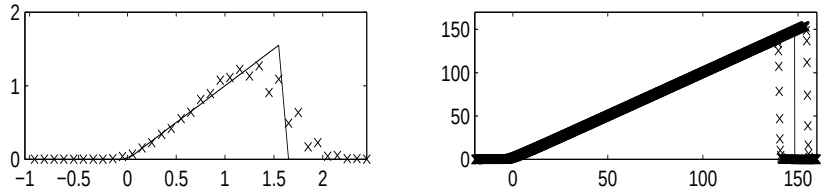

$t = 1$ $t = 10$

Fig. 2. Second order LxF scheme (4.3) for the positive solution (3.14) with $q = 2$. The same phenomenon of separation is observed. The numerical viscosity is smaller.

Unfortunately, the interface approximation given by (4.1) does not satisfy the assumption (3.11). However, one can easily check that the inductive arguments in the proof of Proposition 1 still hold. For example, the key step (3.13) can be replaced by

$$\begin{aligned} U_j^{n+1} &= e^{\Delta t^n}\Big(\frac{1}{2}(CV_{j+1}^n + CV_{j-1}^n) - \frac{\Delta s^n}{2C^{q-1}\Delta x}(f(CV_{j+1}^n) - f(CV_{j-1}^n))\Big) \\ &= e^{\Delta t^n} C\Big(\frac{1}{2}(V_{j+1}^n + V_{j-1}^n) - \frac{\Delta s^n}{2\Delta x}(f(V_{j+1}^n) - f(V_{j-1}^n))\Big) = e^{t^{n+1}} V_j^{n+1}. \end{aligned}$$

Therefore, the assertion of the Proposition 1 is valid for the LxF scheme.

In Figure 1 exact and computed solutions to the reaction-convection equation (2.1) are given using the LxF method. In figures exact and computed solutions are always displayed using lines and dots, respectively. In the figure at time $t = 1$ one can observe a kind of oscillation. However it is not exactly an oscillation. It is a separation. In the scheme (4.2) only odd numbered cells are used to compute the even numbered ones. Hence even numbered grids and odd numbered ones generate two different solutions. In the figure at time $t = 10$ we may clearly observe a separation of two N-waves.

High resolution central schemes were proposed by Nessyahu and Tadmor in 1990 in [17], which is based on the Lax-Friedrichs method. Modified from the LxF scheme using Van Leer's MUSCL-type interpolant [21] a direct second

order modification of LxF scheme for (2.1) can be written as

$$\begin{aligned} U_j^{n+1/2} &= U_j^n - \tfrac{\Delta t^n}{2\Delta x} f'_j \\ U_{j+1}^{n+1} &= e^{\Delta t^n}\Big(\tfrac{1}{2}[U_{j-1}^n + U_{j+1}^n] - \tfrac{1}{4}[U'_{j-1} - U'_{j+1}] - \tfrac{\Delta t^n}{2\Delta x}[f(U_{j+1}^{n+1/2}) - f(U_{j-1}^{n+1/2})]\Big), \end{aligned} \tag{4.3}$$

where the numerical derivatives of the flux $\frac{1}{\Delta x} f'_j = f(u)_x|_{u=U_j} + O(\Delta x)$ and of the solution $\frac{1}{\Delta x} U'_j = u_x|_{u=U_j} + O(\Delta x)$ are given by

$$U'_j = \text{minmod}(\alpha \Delta U_{j-1/2}, \frac{1}{2}(U_{j+1} - U_j), \alpha \Delta U_{j+1/2}), \tag{4.4}$$

$$f'_j = \text{minmod}(\alpha \Delta f_{j-1/2}, \frac{1}{2}(f_{j+1} - f_j), \alpha \Delta f_{j+1/2}), \tag{4.5}$$

where $\alpha \in [1, 2]$, $\Delta U_{j+1/2} = U_{j+1} - U_j$ and

$$\text{minmod}(x_1, x_2, \cdots) = \begin{cases} \min_j\{x_j\} & \text{if } x_j > 0 \text{ for all } j, \\ \max_j\{x_j\} & \text{if } x_j < 0 \text{ for all } j, \\ 0 & \text{otherwise.} \end{cases} \tag{4.6}$$

In Figure 2 exact and computed solutions are similarly presented using this second order LxF scheme. In this example we observe the same phenomenon of separation. The reason of this separation is also based on the fact that only the odd numbered cells are used to compute even numbered cell average of the next time level in the scheme (4.3). To avoid such a separation both of even numbered and odd numbered cells should be used. Therefore considering a staggering scheme in Section 6 is a natural recipe to fix this kind of phenomenon.

5 MacCormack and Lax-Wendroff

In this section we consider two oscillatory second order schemes. In the MacCormack's method the numerical flux at the interface is given by

$$f(u_{j+1/2}^n) = \frac{1}{2}\Big(f(U_{j+1}^n) - f(U_j^n - \frac{\Delta t^n}{\Delta x}[f(U_{j+1}^n) - f(U_j^n)])\Big). \tag{5.1}$$

First we check that this interface approximation does not satisfy the assumption (3.11). Let $U_j^n = CV_j^n$. Then, for $C = e^{t^n} > 1$ and $q > 1$,

$$
\begin{aligned}
f(u^n_{j+1/2}) &= \frac{1}{2}\Big(f(CV^n_{j+1}) - f(CV^n_j - \frac{\Delta t^n}{\Delta x}[f(U^n_{j+1}) - f(U^n_j)])\Big) \\
&= \frac{C^q}{2}\Big(f(V^n_{j+1}) - f(V^n_j - \frac{\Delta t^n}{\Delta x}C^{-1}[f(U^n_{j+1}) - f(U^n_j)])\Big) \\
&= \frac{C^q}{2}\Big(f(V^n_{j+1}) - f(V^n_j - \frac{\Delta t^n}{\Delta x}C^{q-1}[f(V^n_{j+1}) - f(V^n_j)])\Big).
\end{aligned}
$$

However, since

$$
f(Cv^n_{j+1/2}) = C^q f(v^n_{j+1/2}) = \frac{C^q}{2}\Big(f(V^n_{j+1}) - f(V^n_j - \frac{\Delta t^n}{\Delta x}[f(V^n_{j+1}) - f(V^n_j)])\Big),
$$

$u^n_{j+1/2} - Cv^n_{j+1/2} \neq 0$ in general. Now we show that the order of this difference is less than the order of $Cv^n_{j+1/2}$, which implies that at least the leading order part of the interface approximation of the MacCormack's method satisfies the assumption on the interface approximation (3.11).

Here we consider the Burgers case $q = 2$ for simplicity. From the mean value theorem, there exists ξ between $V^n_j - \frac{\Delta t^n}{\Delta x}[f(V^n_{j+1}) - f(V^n_j)]$ and $V^n_j - \frac{\Delta t^n}{\Delta x}C^1[f(V^n_{j+1}) - f(V^n_j)]$ such that

$$
\begin{aligned}
|f(u^n_{j+1/2}) - C^2 f(v^n_{j+1/2})| &= \frac{C^2}{2}(C-1)\frac{\Delta t^n}{\Delta x}\Big|\,[f(V^n_{j+1}) - f(V^n_j)]f'(\xi)\Big| \\
&\leq \frac{\Delta t^n}{2\Delta x}\Big|[f(U^n_{j+1}) - f(U^n_j)]f'(C\xi))\Big|.
\end{aligned}
$$

Employing the exact solutions in (2.8) and the mean value theorem again, we obtain $x_0 \in (x_j, x_j + h)$ such that

$$
|f(U^n_{j+1}) - f(U^n_j)| \cong \frac{1}{2}\Big|(x_j + \Delta x)^2 - x_j^2\Big| \cong \Delta x|x_0| \leq \Delta x \max_j |U^n_j|.
$$

From the exact solution in (2.8) with $q = 2$ we can easily see that $\max_j |U^n_j| = O(e^{t/2}) = O(C^{1/2})$. Since $C\xi$ is between $U^n_j - \frac{\Delta t^n}{\Delta x}C^{-1}[f(U^n_{j+1}) - f(U^n_j)]$ and $U^n_j - \frac{\Delta t^n}{\Delta x}[f(U^n_{j+1}) - f(U^n_j)]$, $f'(C\xi)$ is of order $O(C^{1/2})$. Therefore, since $f(u^n_{j+1/2})$ is of order C, we obtain

$$
\frac{|f(u^n_{j+1/2}) - C^2 f(v^n_{j+1/2})|}{|f(u^n_{j+1/2})|} = O(\Delta x). \tag{5.2}
$$

This estimate indicates that, even if the assumption (3.11) does not hold for the MacCormack's scheme, its leading order approximation satisfies the assumption.

Now we examine the properties of MacCormack's method from numerical experiments. In Figure 3 exact and computed solutions to the reaction-convection

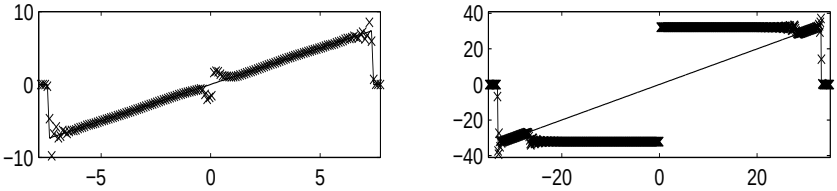

$t = 4$ $t = 7$

Fig. 3. MacCormack's scheme, (3.9) with (5.1), for the sign-changing solution (3.16) with $q = 2$. A non-physical shock emerges from the sign-changing point and finally destroys the computed solution completely.

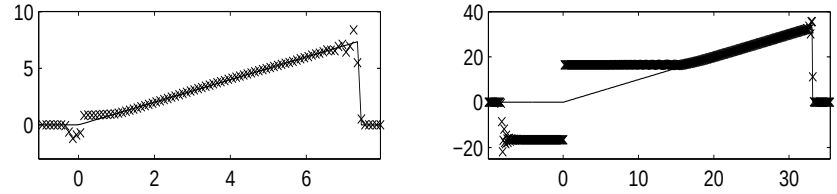

$t = 4$ $t = 7$

Fig. 4. MacCormack's scheme for the positive solution (3.14) with $q = 2$. Even for this positive case the similar non-physical shock appears due to the oscillation.

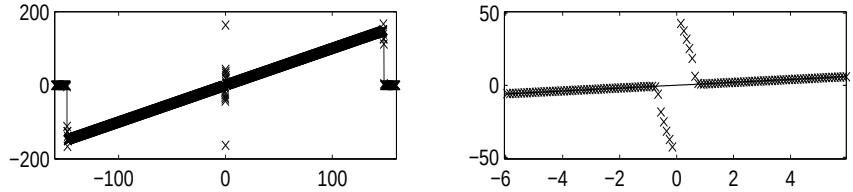

Fig. 5. Richtmyer two-step Lax-Wendroff scheme, (3.9) with (5.3), at time $t = 10$. Non-physical blowup appears at the sonic point and the computed solution collapse.

equation (2.1) are given using the fully discrete method (3.9) with the MacCormack's numerical flux (5.1). In the figure at time $t = 4$ one can observe a small discontinuity that violates the entropy condition (2.3). This non-physical shock grows fast and eventually all the meaningful information of the solution disappears. (See the figure at $t = 7$.)

Proposition 1 claims that this strange behavior of the numerical experiment is due to the property of the scheme for the convection equation (3.1). In fact this behavior is related to the well known fact of the MacCormack's scheme that for any $c > 0$ the discrete function

$$U_j^n = \begin{cases} -c, & j \le 0 \\ c, & j > 0 \end{cases}$$

is a steady state of the MacCormack's scheme for the convection equation (2.9). This example indicates that this kind of steady state is not a rare case

and one should deal with such a blowup if reaction terms play a crucial role. In fact, since the approximation is a piecewise constant function, such a discontinuity may appear easily across a sign-changing point. Furthermore, even for a positive solution case this kind of inadmissible discontinuity may appear due to the oscillating property of the scheme. In Figure 4 we may observe a non-physical shock developed from a positive solution.

Next we consider the Richtmyer two-step Lax-Wendroff method. In this scheme the interface approximation is given by

$$u^n_{j+1/2} = \frac{1}{2}(U^n_j + U^n_{j+1}) - \frac{\Delta t^n}{2\Delta x}[f(U^n_{j+1}) - f(U^n_j)]. \tag{5.3}$$

As we did for the MacCormack's scheme we can similarly show that at least the leading order term satisfies the assumption (3.11). In Figure 5 computed solutions of this scheme is given together with exact ones. The numerical solution looks fine until $t = 9$. However, when it reaches $t = 10$, we can observe a nonphysical pick around the sign changing point and the computed solution blows up quickly.

Similar behaviors of computed solutions are observed with other powers $q > 1$. One may observe such blowups more easily for the periodic cases (3.18).

6 Modified schemes based on LxF

The separation into two waves of computed solutions in Figures 1 and 2 is due to the separation of even numbered cells and odd numbered ones in their schemes (4.2) and (4.3). Therefore the best way to cure such a symptom is to consider a scheme in staggered form. In this section we consider several modified schemes introduced in [5]. A staggered form of the LxF scheme for the convection-reaction equation (2.1) can be written as

$$U^{n+1}_{j+1/2} = e^{\Delta t^n}\Big(\frac{1}{2}[U^n_j + U^n_{j+1}] - \frac{\Delta t^n}{2\Delta x}[f(U^n_{j+1}) - f(U^n_j)]\Big). \tag{6.1}$$

To eliminate the inconvenience of staggering schemes one may consider the average of two neighboring staggered cell-averages to construct a nonstaggering scheme,

$$U^{n+1}_j = e^{\Delta t^n}\Big(\frac{1}{4}(U^n_{j+1} + 2U^n_j + U^n_{j-1}) - \frac{\Delta t^n}{2\Delta x}(f(U^n_{j+1}) - f(U^n_{j-1}))\ \Big). \tag{6.2}$$

The second order modification (4.3) can be also written in a staggered form:

$$U^{n+1}_{j+1/2} = \frac{1}{2}[U^n_j + U^n_{j+1}] + \frac{1}{8}[U'_j - U'_{j+1}] - \frac{\Delta t^n}{\Delta x}[f(U^{n+1/2}_{j+1}) - f(U^{n+1/2}_j)], \quad (6.3)$$

where U'_j and $U^{n+1/2}_j$ are same as the ones in Section 4 given by (4.3)–(4.6). This scheme is usually called the NT scheme and is employed in this section for numerical computations. We can similarly construct a nonstaggering scheme based on the NT scheme,

$$\begin{aligned} U^{n+1}_{j+1} = e^{\Delta t^n}\Big(& \tfrac{1}{4}[U^n_{j-1} + 2U^n_j + U^n_{j+1}] + \tfrac{1}{16}[U'_{j-1} - U'_{j+1}] \\ & -\tfrac{\lambda_n}{2}[f(U^{n+1/2}_{j+1}) - f(U^{n+1/2}_{j-1})] - \tfrac{1}{8}[U'_{j+1/2} - U'_{j-1/2}]\Big), \end{aligned} \quad (6.4)$$

where

$$U'_{j+1/2} = \text{minmod}(U^{n+1}_{j+3/2} - U^{n+1}_{j+1/2}, U^{n+1}_{j+1/2} - U^{n+1}_{j-1/2})$$

and $U^{n+1}_{j+1/2}$ is given by the staggered method (6.3).

These schemes do not exhibit such bizarre behaviors as the ones observed in previous two sections. Therefore discussing the accuracy of the scheme is now meaningful. First we compare the shock estimation. In Figures 6 and 7 computed solutions of the NT scheme are given for the positive N-wave (3.14) and the sign-changing N-wave (3.16), respectively. In the figures solutions are plotted near the shock to check the performance. Most of the cases the NT scheme provides reasonably correct shock locations. The only exception is the case for the sign-changing case with $q = 3$. In this case the numerical solution gives slow shock propagation. This behavior seems related to the numerical viscosity and the singularity of the solution near the sign change.

Computed solutions for the roll wave (3.18) with the periodic boundary condition show how the scheme approximates the rarefaction wave. In the first row of Figure 8 computed solutions are given with exact ones using the NT scheme (6.3). In the second row the error of computed solutions are given. Since the computed solution is an approximation of cell averages under the initial discretization (3.19), the error is taken as

$$Error = U^n_j - \int_j^{j+1} u(x, t^n)dx, \quad (6.5)$$

where u is the exact solution. In the figures this error is plotted at the grid point $x_{j+1/2}$. From the graph of the error in the second row we observe that the error is an increasing function away from discontinuities for all three cases. This implies that the graph of the approximation is steeper and hence the

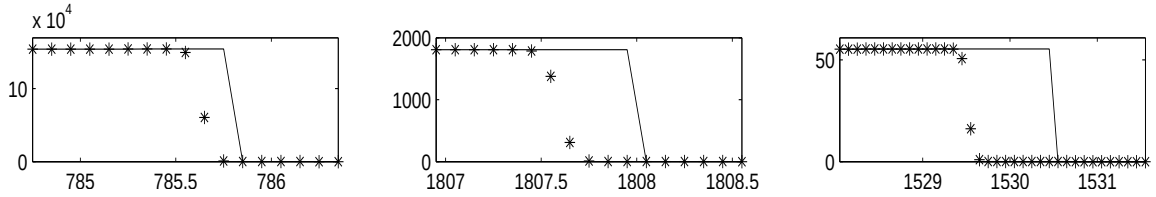

$q = 1.5,\ t = 20$ $q = 2,\ t = 15$ $q = 3,\ t = 11$

Fig. 6. NT scheme (6.3) for the positive solution (3.14). The magnifications of computed solution near the shock show reasonably correct shock locations.

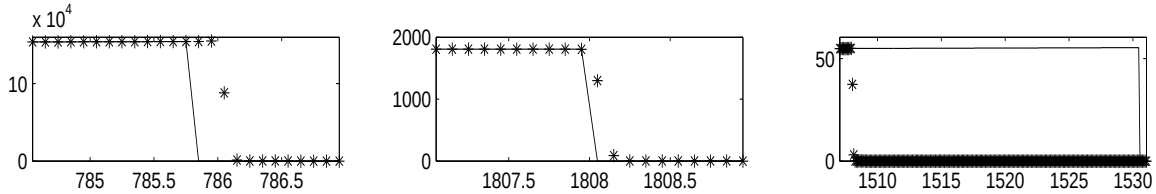

$q = 1.5,\ t = 20$ $q = 2,\ t = 15$ $q = 3,\ t = 11$

Fig. 7. NT scheme for the sign changing solution (3.16). Shock locations are correct except the case $q = 3$ when the exact solution has a singularity at the origin.

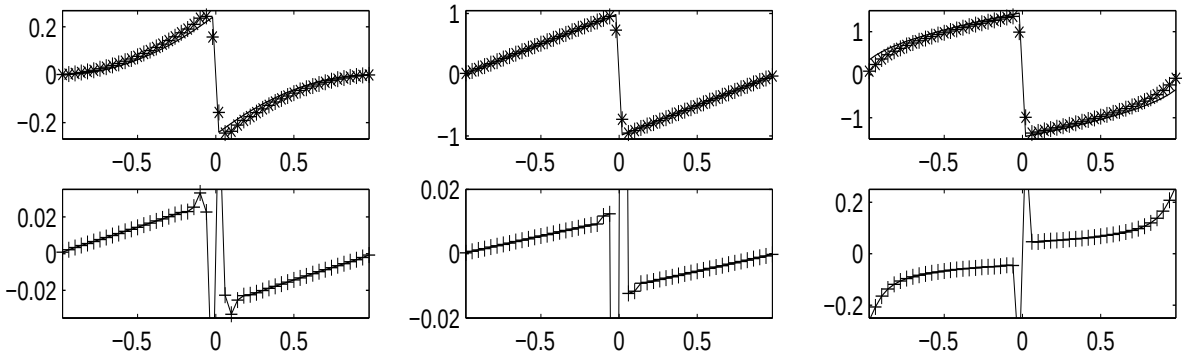

$q = 1.5$ $q = 2$ $q = 3$

Fig. 8. NT scheme for the periodic solution (3.18). The error in the second row is an increasing function away from the shock. There is no sonic glitch. The discontinuity at the sonic point $x = \pm 1$ for the case $q = 3$ is due to the singularity of the exact solution.

numerical flux is slightly weaker than the exact one. We may also say that the sonic glitch phenomenon is not observed from all of three cases. The numerical error for the case $q = 3$ shows a discontinuity at the sonic points. Notice that the continuity is simply due to the singularity of the exact solution at the sonic point.

Remark 2 *Note that the linear reaction term makes the solution grow and the nonlinear convection term makes it flat. Therefore, if the error function in (6.5) increases away from the discontinuity (i.e., the computed solution is flatter than the exact one), then we may say that the flux is overestimated numerically. Another factor that decides the signs of the error function is so called the sonic glitch phenomenon. Note that* $x = \pm 1$ *are sonic points*

for the periodic cases. Certain numerical schemes generate entropy violating discontinuities at such points, which is called a sonic glitch.

Next we consider one more central scheme which also has the property of Godunov scheme. In [9,10] a Godunov-type semi-discrete central scheme (NTK scheme for short) was introduced. This scheme is constructed based on a piecewise linear approximation like the NT scheme. We compute the local speeds of propagation at the interface $x = x_{j+1/2}$ which may have discontinuities. Since the speed of propagation is related to the CFL condition, we can estimate the local speeds of the right and left side at the cell boundary. The local speeds of wave propagation are bounded by $a^n_{j+1/2,r}$ and $a^n_{j+1/2,l}$ which are given by

$$a^n_{j+1/2,r} = \max_{\mathcal{C}}(f'(u), 0) \quad , \quad a^n_{j+1/2,l} = \min_{\mathcal{C}}(f'(u), 0), \tag{6.6}$$

where $\mathcal{C}$ is a relevant range for u. Employing this local speed of propagation the flux at the interface is approximated by

$$\begin{aligned} f(u^n_{j+1/2}) = & \frac{a_{j+1/2,r} f(u^-_{j+1/2}) - a_{j+1/2,l} f(u^+_{j+1/2})}{a_{j+1/2,r} - a_{j+1/2,l}} \\ & + \frac{a_{j+1/2,r} a_{j+1/2,l}}{a_{j+1/2,r} - a_{j+1/2,l}} [u^+_{j+1/2} - u^-_{j+1/2}], \end{aligned} \tag{6.7}$$

where $u^+_{j+1/2}$ and $u^-_{j+1/2}$ are computed as

$$\begin{aligned} & u^+_{j+1/2} \equiv U^n_{j+1} - \frac{\Delta x}{2}(u_x)_{j+1}(t^n), \\ & u^-_{j+1/2} \equiv U^n_j + \frac{\Delta x}{2}(u_x)_j(t^n), \\ & (u_x)_j = \text{minmod}(\alpha \frac{U^n_{j+1} - U^n_j}{\Delta x}, \frac{U^n_{j+1} - U^n_{j-1}}{\Delta x}, \alpha \frac{U^n_j - U^n_{j-1}}{\Delta x}), \quad 1 \le \alpha \le 2. \end{aligned}$$

From Figures 9 and 10 one may observe that the NTK scheme provides pretty correct shock approximation except the sign-changing case with $q = 3$. In this case the shock location of the NTK scheme is about the middle of the ones of the NT scheme and of the exact solution. Considering the fact that the Godunov scheme provides almost exact shock location for this case (see Figures 13) we may feel that the NTK scheme is placed between the NT scheme and the Godunov scheme.

In Figure 11 computed solutions of the roll wave (3.18) are given together with the exact ones and error functions. First we may observe sonic glitches for the case $q = 2$ and $q = 3$ which is a property of the Godunov scheme. The

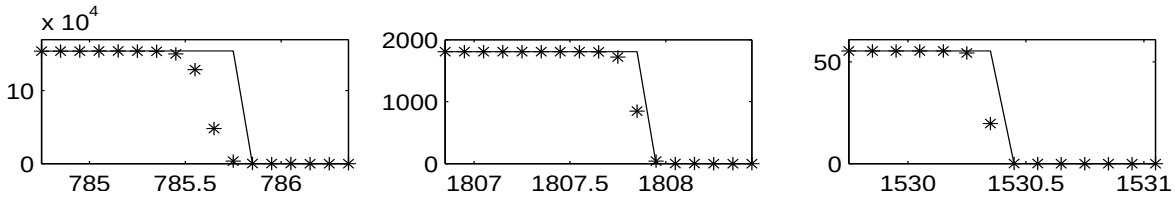

$q = 1.5,\ t = 20$ $q = 2,\ t = 15$ $q = 3,\ t = 11$

Fig. 9. NTK scheme, (3.10) with (6.7), for the positive solution (3.14). The method provides correct shock locations.

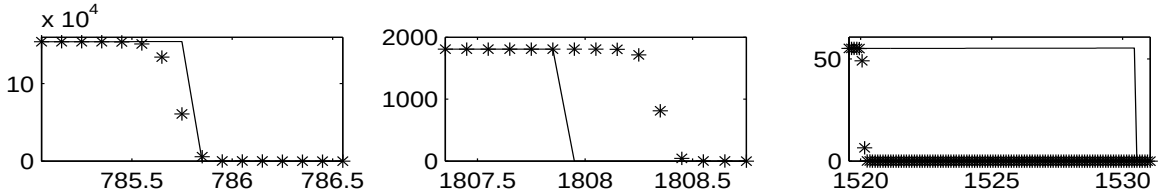

$q = 1.5,\ t = 20$ $q = 2,\ t = 15$ $q = 3,\ t = 11$

Fig. 10. NTK scheme for the sign changing solution (3.16). Shock locations are correct except the case $q = 3$ due to the singularity at the sonic point.

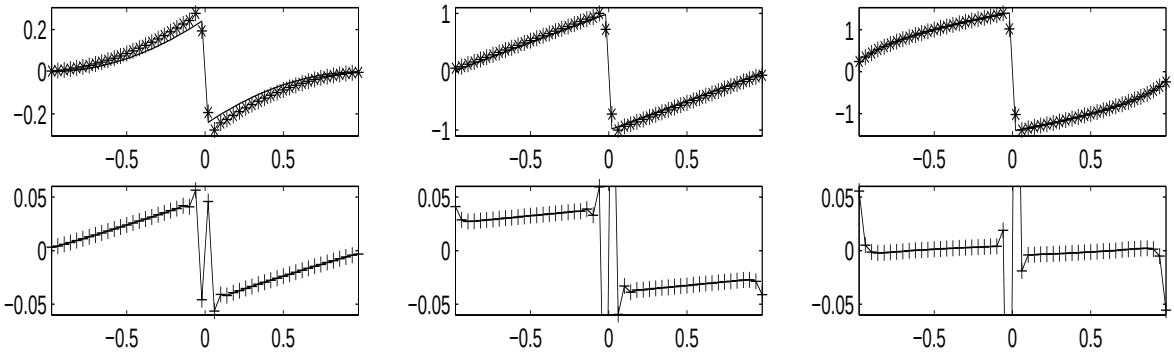

$q = 1.5$ $q = 2$ $q = 3$

Fig. 11. NTK scheme for the periodic solution (3.18). The error functions are increasing in all three cases away from the shock. Sonic glitches are observed if $q = 2$ or 3.

error is an increasing away from the discontinuity and the sonic point which is a property of the NT scheme.

7 Godunov method

Godunov schemes [1,11] are based on either the exact or an approximate solution of the Riemann problem using characteristic information within the framework of a conservative method. Since the flux is convex $f''(u) > 0$, the interface approximation of the first order Godunov method is simply given by

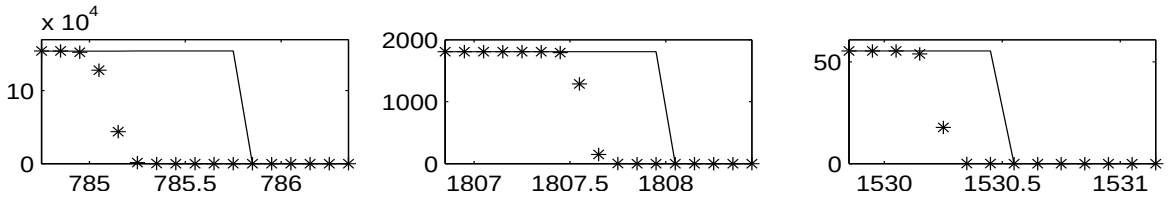

$q = 1.5,\ t = 20$ $\qquad$ $q = 2,\ t = 15$ $\qquad$ $q = 3,\ t = 11$

Fig. 12. The first order Godunov scheme, (3.9) with (7.1), for the positive solution (3.14). The shock locations are reasonably correct even with this first order scheme.

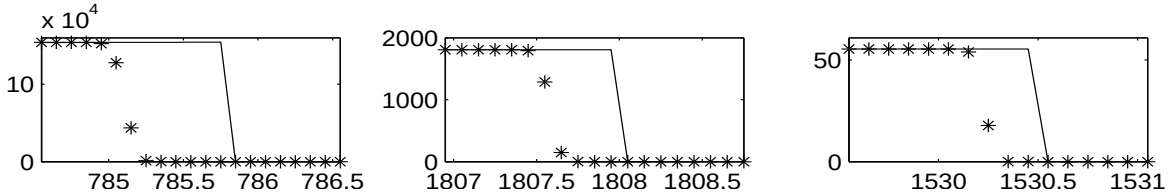

$q = 1.5,\ t = 20$ $\qquad$ $q = 2,\ t = 15$ $\qquad$ $q = 3,\ t = 11$

Fig. 13. The first order Godunov scheme for the sign changing solution (3.16). The shock locations are correct even for the singular case $q = 3$.

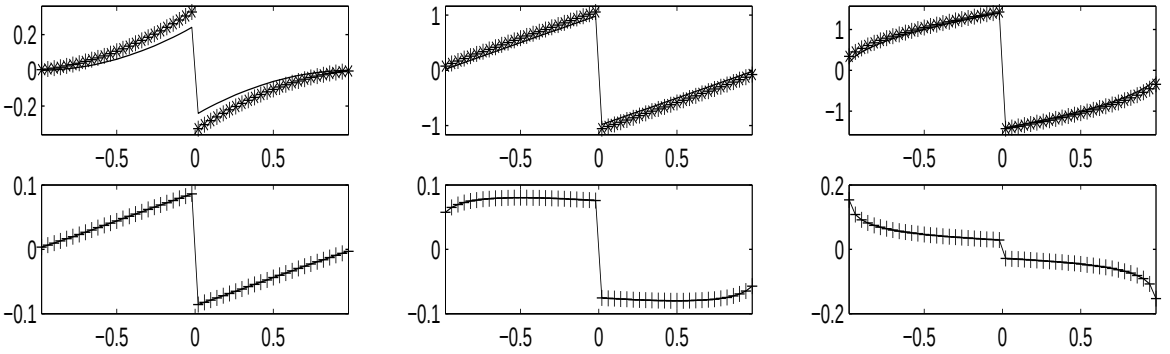

$q = 1.5$ $\qquad$ $q = 2$ $\qquad$ $q = 3$

Fig. 14. The first order Godunov scheme for the periodic solution (3.18). Sonic glitches are observed for $q = 2, 3$. The error increases if $q = 1.5$ or 2, but decreases if $q = 3$. Godunov is the only scheme with a decreasing error function in our tests.

$$u^n_{j+1/2} = \begin{cases} U_j & \text{if } U_j > 0 \text{ and } s > 0, \\ U_{j+1} & \text{if } U_{j+1} < 0 \text{ and } s < 0, \\ 0 & \text{if } U_j < 0 < U_{j+1}. \end{cases} \tag{7.1}$$

Here, $s = [f(U_{i+1}) - f(U_i)]/(U_{i+1} - U_i)$ is the shock speed at the interface $x_{j+1/2}$. Clearly, this interface approximation satisfies the condition (3.11) and the assertion in Proposition 1 is valid.

In Figures 12 and 13 computed solutions of the first order Godunov scheme are given for the positive N-wave (3.14) and the sign-changing N-wave (3.16), respectively. One can observe that the Godunov method gives equally correct

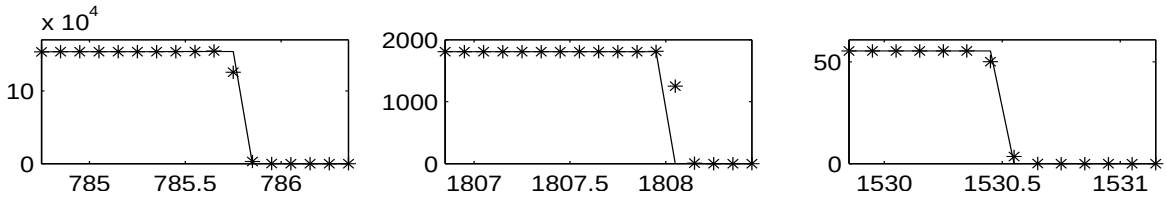

$q = 1.5,\ t = 20$ $q = 2,\ t = 15$ $q = 3,\ t = 11$

Fig. 15. The second order Godunov (CLAWPACK) for the positive solution (3.14). The shock locations are almost exact for all of three cases.

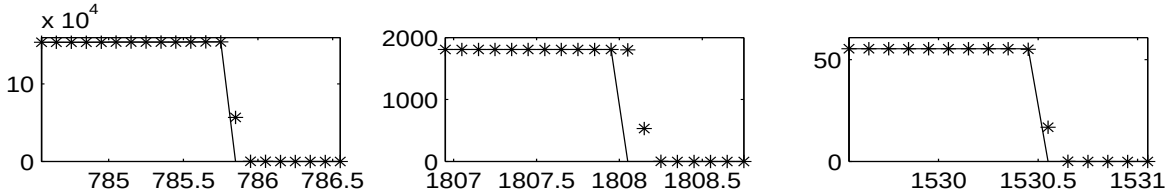

$q = 1.5,\ t = 20$ $q = 2,\ t = 15$ $q = 3,\ t = 11$

Fig. 16. The second order Godunov for the sign changing solution (3.16). The shock locations are almost exact even for the singular case $q = 3$.

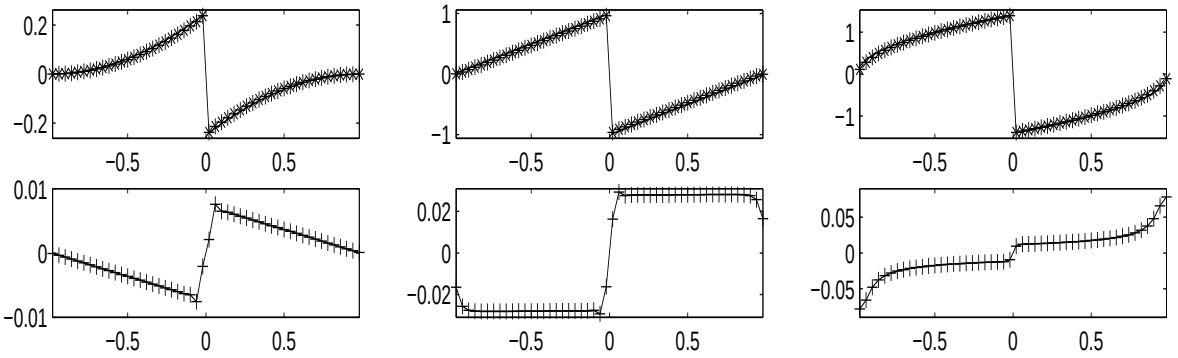

$q = 1.5$ $q = 2$ $q = 3$

Fig. 17. The second order Godunov for the periodic solution (3.18). The sonic glitch is observed for the case $q = 2$. The error function decreases for the case $q = 1.5$.

shock location for both of positive and sign-changing cases. In particular the shock location is pretty correct even for the sign-changing case with $q = 3$ which is the case that all the other schemes considered give pretty poor performance.

In the first row of Figure 14 computed solutions for the roll wave case are given with the exact ones. The computed errors are given in the second row. First we may observe sonic glitches for the cases $q = 2$ and $q = 3$. For the case $q = 1.5$ the rarefaction wave has slope zero at the sonic point and it seems the reason that a glitch does not develop. Another special property of the scheme is that the error is decreasing for the case $q = 3$. So far all the error functions are increasing and hence this is the first example with overestimated numerical flux.

The Godunov method can be modified to a second order scheme by employing proper limiter. For this example we simply use the CLAWPACK [13] with monotonized centered limiter. From Figures 15 and 16 one can observe that this second order Godunov scheme provide very accurate shock location for all of six cases. It is almost exact. Considering the poor performance of other schemes for the sign-changing case with $q = 3$, this scheme is exceptionally good.

On the other hand, from Figure 17, one may observe a funny phenomenon. First the sonic glitch is observed for the case $q = 3$. For the case $q = 2$ the discontinuity observed satisfies the entropy condition. Therefore, it is hard to call it a glitch. For this case there is no singularity in the solution. So it is hard to explain why it happens. The overall error is smaller than most of other schemes or is competitive with others at least. However the error function is decreasing for the case $q = 1.5$ and is increasing for the case $q = 3$. The case $q = 2$ is somewhat between of them. So $q = 1.5$ is the case that the flux is over estimated numerically even if the size is small. Note that the property of the scheme is also strongly depending on the property of the limiter. Using different limiter one may obtain different phenomenon.

8 WENO

The last numerical scheme considered is a high-order accurate weighted essentially non-oscillatory (WENO for short) method (see [4,2,6,15,18]). For this example we employ the semi-discrete Runge-Kutta type method (3.10). To avoid entropy violating solutions and obtain the numerical stability we split the flux $f(u)$ into two components f^+ and f^- such that

$$f(u) = f^+(u) + f^-(u), \tag{8.1}$$

where $\frac{\partial f^+}{\partial u} \geq 0$ and $\frac{\partial f^-}{\partial u} \leq 0$. One of the simplest flux splitting is the Lax-Friedrichs splitting which is given by

$$f^{\pm}(u) = \frac{1}{2}(f(u) \pm \alpha u), \tag{8.2}$$

where $\alpha = \max_u |f'(u)|$ over the pertinent range of u which can be decided a-priori using the explicit formula for the exact solution.

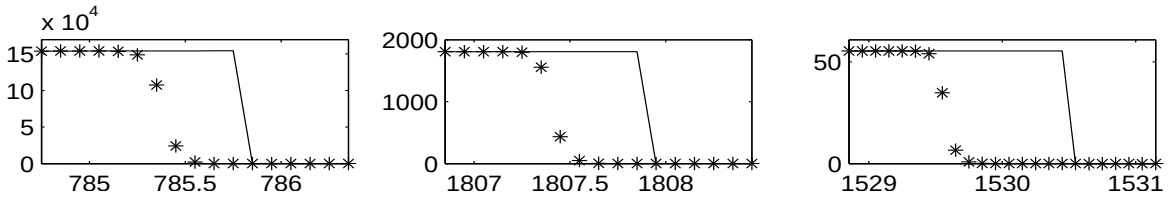

$q = 1.5,\ t = 20$ $q = 2,\ t = 15$ $q = 3,\ t = 11$

Fig. 18. WENO scheme, (3.10) with (8.3), for the positive solution (3.14). This method provides reasonably correct shock locations.

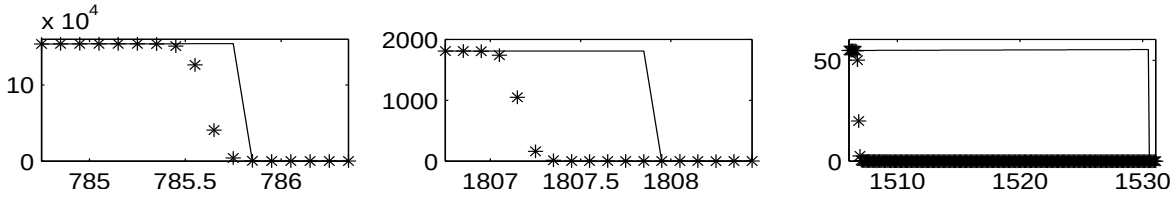

$q = 1.5,\ t = 20$ $q = 2,\ t = 15$ $q = 3,\ t = 11$

Fig. 19. WENO scheme for the sign changing solution (3.16). Shock locations are correct except the case $q = 3$ due to the singularity at the sonic point.

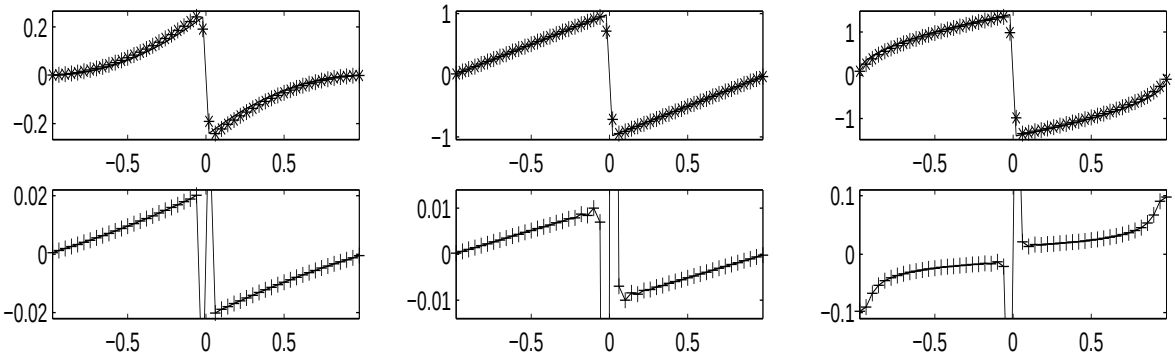

Fig. 20. WENO scheme for the periodic solution (3.18). The error functions are increasing. There is no sonic glitch. The discontinuity at the sonic point for the case $q = 3$ is due to the singularity of the exact solution at the sonic point.

The interface approximation of the fifth order WENO with Lax-Friedrichs splitting (WENO-LF for short) is given by

$$\begin{aligned} f(u^n_{j+1/2}) = \tfrac{1}{12}(-f_{j-1} + 7f_j + 7f_{j+1} - f_{j+2}) - \Phi_N(\Delta f^+_{j-\frac{3}{2}}, \Delta f^+_{j-\frac{1}{2}}, \Delta f^+_{j+\frac{1}{2}}, \Delta f^+_{j+\frac{3}{2}}) \\ + \ \Phi_N(\Delta f^-_{j+\frac{5}{2}}, \Delta f^-_{j+\frac{3}{2}}, \Delta f^-_{j+\frac{1}{2}}, \Delta f^-_{j-\frac{1}{2}}), \end{aligned} \tag{8.3}$$

where $f_j = f(u^n_j)$, $f^\pm_j = f^\pm(u^n_j)$, $\Delta f^\pm_{i+\frac{1}{2}} = f^\pm_{i+1} - f^\pm_i$ and

$$\Phi_N(a, b, c, d) = \frac{1}{3}\omega_0(a - 2b + c) + \frac{1}{6}(\omega_2 - \frac{1}{2})(b - 2c + d). \tag{8.4}$$

The nonlinear weights ω_0 and ω_2 are defined by

$$\omega_j = \frac{\alpha_j}{\sum_{l=0}^{k-1} \alpha_l} , \quad \alpha_l = \frac{d_l}{(\varepsilon + \beta_l)^2} , \quad d_0 = \frac{1}{10} , \quad d_1 = \frac{3}{5} , \quad d_2 = \frac{3}{10} ,$$

where $0 < \varepsilon \ll 1$ is taken to prevent singularity and the smoothness indicators β_j's are given by

$$\begin{aligned} \beta_0 &= \tfrac{13}{12}(f_{i-2} - 2f_{i-1} + f_i)^2 + \tfrac{1}{4}(f_{i-2} - 4f_{i-1} + 3f_i)^2 \\ \beta_1 &= \tfrac{13}{12}(f_{i-1} - 2f_i + f_{i+1})^2 + \tfrac{1}{4}(f_{i-1} - f_{i+1})^2 \\ \beta_2 &= \tfrac{13}{12}(f_i - 2f_{i+1} + f_{i+2})^2 + \tfrac{1}{4}(3f_i - 4f_{i+1} + f_{i+2})^2. \end{aligned} \tag{8.5}$$

In Figures 18 and 19 computed solutions of the WENO-LF scheme for the solutions (3.14) and (3.16) are given using Rung-Kutta time discretization (3.10). The scheme gives reasonable shock location except the case $q = 3$ for the sign-changing solution. In this case the shock location is pretty same as the NT scheme. In the roll wave computation, Figure 20, the sonic glitch is not observed. In all of three cases the error functions are increasing except near the shock place. Therefore, we may say that the flux is slightly under estimated.

References

[1] S.K. Godunov, *A difference method for numerical calculation of discontinuous solutions of the equations of hydrodynamics*. Mat. Sb. (N.S.) 47 (1959) 271–306.

[2] Y. Ha, C. L. Gardner, A. Gelb and C.-W. Shu, *Numerical Simulation of High Mach Number Astrophysical Jets with Radiative Cooling*. Journal of Scientific Computing, 24 (2005) 29–44.

[3] Y. Ha and Y.-J. Kim, *Comparison of numerical schemes for a convection reaction equations*. preprint.

[4] A. Harten, B. Engquist, S. Osher and S. Chakravarthy, *Uniformly high order essentially non-oscillatory schemes,III* . J. Comput. Phys., 231 (1987) 231–303.

[5] G.-S. Jiang, D. Levy, C.-T. Lin, S. Osher and E. Tadmor, *High-resolution nonoscillatory central schemes with nonstaggered grids for hyperbolic conservation laws*. SIAM J. Numer. Anal., 35 (1998) 2147–2168.

[6] G.-S. Jiang, C.-W. Shu, *Efficient Implementation of Weighted ENO schemes*, J. Comput. Phys., 126 (1996) 202–228.

[7] S. Jin and M. Katsoulakis, *Hyperbolic systems with supercharacteristic relaxations and roll waves*, SIAM J. Appl. Math. 61 (2000) 271–292

[8] S. Jin and Y.-J. Kim, *On the computation of roll waves*, M2AN Math. Model. Numer. Anal. 35 (2001), no. 3 463–480.

[9] A. Kurganov, S. Noelle and G. Petrova, *Semi-discrete central-upwind schemes for hyperbolic conservation laws and Hamilton-Jacobi equations*, SIAM J. Sci. Compu. ,23 (2001) 703-740.

[10] A. Kurganov, and E. Tadmor, *New high-resolution central schemes for nonlinear conservation laws and convection-diffusion equations*, J. Comput. Phys. 160 (2000) 241-282.

[11] R.J. LeVeque, *Numerical methods for conservation laws*, Lectures in Mathematics ETH Zürich, Birkhäuser Verlag, Basel, 1990.

[12] R.J. LeVeque, *High-resolution conservative algorithms for advection in incompressible flow*, SIAM J. Numer. Anal., 33(1996) 627–665.

[13] R.J. LeVeque, *Clawpack Version 4.0 Users Guide*, Technical report, University of Washington, Seattle, 1999. Available online at http://www.amath.washington.edu/∼claw/.

[14] R. Liska and B. Wendroff *Comparison of several difference schemes on 1D and 2D test problems for the Euler equations*, SIAM J. Sci. Comput., 25(2003) no. 3 995-1017

[15] X.-D. Liu, S. Osher and T. Chan, *Weighted essentially non-oscillatory schemes*. J. Comput. Phys. 115 (1994) 200–212.

[16] A.N. Lyberopoulos, *Asymptotic oscillations of solutions of scalar conservation laws with convexity under the action of a linear excitation*, Quar. Appl. Math. XLVIII, 755-765, 1990.

[17] H. Nessyahu and E. Tadmor, *Nonoscillatory central differencing for hyperbolic conservation laws*, J. Comput. Phys., 87 (1990) 408–463.

[18] C.-W. Shu and S. Osher, *Efficient implementation of essentially non-oscillatory shock capturing schemes*. J. Comput. Phys. 77 (1988) 439–471.

[19] C.-W. Shu and S. Osher, *Efficient implementation of essentially non-oscillatory shock capturing schemes, II*. J. Comput. Phys. 83 (1989) 32–78.

[20] C.-W. Shu and S. Osher, *Essentially non-oscillatory and weighted essentially non-oscillatory schemes for hyperbolic conservation laws, in Advanced Numerical Approximation of Nonlinear Hyperbolic Equations, B. Cockburn, C. Johnson, C.-W. Shu and E. Tadmor (Editor: A.Quarteroni).*, Lecture Notes in Mathematics, volume 1697, Springer, 325 (1998)

[21] B. van Leer, *MUSCL, A New Approach to Numerical Gas Dynamics.* In Computing in Plasma Physics and Astrophysics, Max-Planck-Institut fűr Plasma Physik, Garchung, Germany, April 1976.